applied sciences

Article

Inkjet-Printed Flexible Strain-Gauge Sensor on Polymer Substrate: Topographical Analysis of Sensitivity

Hyunkyoo Kang [1,*], Seokjin Kim [1], Jaehak Shin [2] and Sunglim Ko [2]

1 Department of Mechatronics Engineering, Konkuk University Glocal Campus, 268 Chungwondaero, Chungju-si 27478, Korea; seokjin801@kku.ac.kr
2 Department of Mechanical Design and Production Engineering, Konkuk University, 120 Neungdong-ro, Seoul 05029, Korea; dftd93@konkuk.ac.kr (J.S.); slko@konkuk.ac.kr (S.K.)
* Correspondence: hyunkyoo@kku.ac.kr; Tel.: +82-43-840-3626; Fax: +82-43-840-4169

Abstract: Inkjet-printed strain gauges on flexible substrates have recently been investigated for biomedical motion detection as well as the monitoring of structural deformation. This study performed a topographical analysis of an inkjet-printed strain gauge constructed using silver conductive ink on a PET (polyethylene terephthalate) substrate. Serpentine strain-gauge sensors of various thicknesses and widths were fabricated using inkjet printing and oven sintering. The fabricated gauge sensors were attached to curved surfaces, and gauge factors ranging from 2.047 to 3.098 were recorded. We found that the cross-sectional area of the printed strain gauge was proportional to the gauge factor. The correlation was mathematically modelled as $y = 0.4167\ln(x) + 1.3837$, for which the coefficient of determination (R^2) was 0.8383.

Keywords: additive manufacturing; inkjet; printed strain gauge; topography

check for updates

Citation: Kang, H.; Kim, S.; Shin, J.; Ko, S. Inkjet-Printed Flexible Strain-Gauge Sensor on Polymer Substrate: Topographical Analysis of Sensitivity. *Appl. Sci.* **2022**, *12*, 3193. https://doi.org/10.3390/app12063193

Academic Editor: Alfio Dario Grasso

Received: 8 February 2022
Accepted: 10 March 2022
Published: 21 March 2022

1. Introduction

For decades, strain-gauge sensors have been employed to measure forces applied to target objects. A strain gauge is constructed from a conductive substance with a wavy pattern, which is attached to the object under investigation. Deformations induced by applied forces result in variations in the resistance [1,2].

Additive manufacturing using techniques such as inkjet [3], screen [4], aerosol [5], gravure [6,7] and shadow-mask [8] printing have been attracting increasing interest because it is environmentally friendly and material-saving compared with conventional photolithography or chemical vapour deposition. This approach also allows direct printing of the strain gauge onto the surface of the target object without a gluing process, thereby avoiding force decoupling between the substrate and glued strain-gauge material [9].

Highly stretchable as well as highly sensitive strain gauges have recently been used to measure on human motion in biomedical applications [10]. Carbon [11], silver (Ag) nanowires [12], Ag flakes [13], PeDOT:PSS [poly (3,4-ethylenedioxythiophene): poly (styrenesulfonate)] [14] and graphite [15] have been tested as base materials for the conductive strain-gauge pattern.

A full Wheatstone bridge with a single-symmetry structure was suggested for compensating for surrounding temperature variations when performing structural health monitoring outdoors [15]. A parametric design and fabrication process were investigated for developing analytical models and optimized process parameters for a sandwich-layer-structure strain gauge with an insulation layer [16].

How the set-in effect, nonlinear responses and hysteresis influence the signals produced by printed strain gauges has also been investigated [17]. Moreover, a comparison study was carried out between screen-printed strain-gauge sensor with carbon and inkjet-printed sensors with Ag nanoparticles (AgNPs) [18]. The microstructure, gauge factor and long-term repeatability were analyzed. However, none of these studies performed a topographical analysis of inkjet-printed strain gauges constructed using Ag on a polyethylene terephthalate (PET) substrate.

This study used inkjet printing to fabricate serpentine strain-gauge patterns with various thicknesses and widths of the conductive material. The initial resistances, thickness profiles and cross-sectional areas were identified after sintering the printed patterns, and strains were calculated under bending. The correlation between the gauge factor and topography was investigated using both theoretical and experimental approaches.

2. Experimental

2.1. Materials

A commercial particle-free Ag conductive ink (TEC-IJ-060) was purchased (InkTec, Ansan-si, Gyeonggi-do, Korea) whose viscosity, surface tension, density and metal contents are 5~15 mPa.s, 27~32 dynes/cm, 1.03 g/cm^3 and 12 wt% at 25 °C, respectively. An A4-sized heat-stabilized PET substrate (AH71D, SKC, Seoul, Korea) was prepared for ink deposition. The thickness of the substrate was 100 µm.

2.2. Fabrication

A drop-on-demand (DOD) inkjet printer (DMP-2831, Fujifilm Dimatix, Santa Clara, CA, USA) was used to produce the strain-gauge pattern on the substrate. A 10 pL cartridge with 16 nozzles (DMC-11610, Fujifilm Dimatix, Santa Clara, CA, USA) was filled with Ag conductive inks. To ensure stable ink deposition, three nozzles were selected for Ag ink ejection. The nozzle aperture was 21.5 µm. The diameter of a single droplet on the substrate was approximately 51.4 µm, as shown in Figure 1a. Thus, the drop spacing for producing a serpentine pattern was determined as 30 µm to ensure the formation of a continuous line. The finalized pattern design is depicted in Figure 1b. The width, pitch and height of the standard pattern were 140 µm, 700 µm and 7 mm, respectively. The plate with the substrate was placed inside the inkjet printer and heated at 50 °C during the ink deposition, in order to form a stable pattern by the rapid evaporation of the solution. After the printing process, the deposited strain-gauge pattern was sintered in a conventional convection oven (OF-22GW, JEIO Tech, Daejeon, Korea) at 150 °C for 15 min to ensure high conductivity.

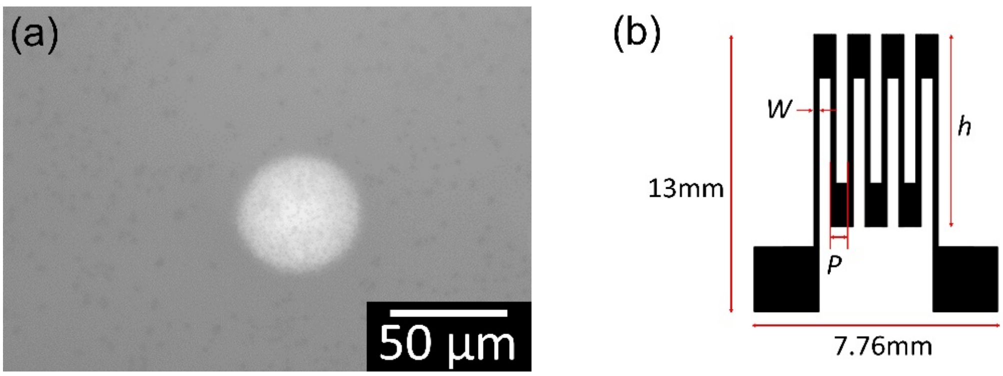

Figure 1. (**a**) Deposited single droplet on the substrate. The droplet diameter was approximately 51.4 µm. (**b**) The designed strain-gauge pattern. *W*, *P* and *h* are the width, pitch and height of the pattern, respectively.

2.3. Characteristics

The electrical characteristics of each printed strain gauge were evaluated by resistance measurements using a source meter (2400, Keithley, Solon, OH, USA). The sensitivity of the strain gauge was quantified as the gauge factor (G_f), which was defined as the ratio of the electrical resistance change induced by the applied strain, as in Equation (1). A specified strain was applied to the printed strain-gauge pattern by bending it. Five fan-shaped pillars with various curved surfaces were manufactured using a commercial three-dimensional (3D) printer, as shown in Figure 2. Then, the printed strain-gauge pattern was attached to each curved surface to measure the electrical resistance under bending. The strain on the printed pattern induced by bending was calculated using Equation (2) [19]

$$G_f = (\Delta R / R_0)/\varepsilon \quad (1)$$

$$\varepsilon = c/\rho \quad (2)$$

where G_f, ε, c, ρ, ΔR, R_0 are the gauge factor, the strain, half the substrate thickness, the bending curvature, the change in resistance and the initial resistance, respectively.

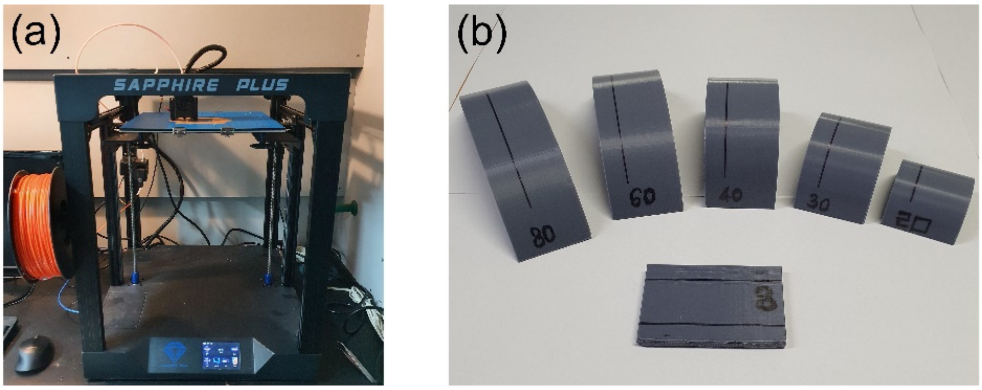

Figure 2. (**a**) Three-dimensional printer. (**b**) Three-dimensionally printed pillars with various arc-shaped cross sections.

For the topographical analysis of the printed strain-gauge sensor, specimens were prepared using two approaches: stacked and expanded. For the stacked approach, the serpentine pattern was overprinted on the same position of the substrate, and three kinds of specimens were fabricated: single layer, three layers and five layers. For the expanded approach, thin, normal-width and double-width patterns were produced using two, four and seven droplets, respectively. In all cases, the drop spacing was fixed at 30 μm. An interferometer (Nanoscan NS-E1000, Nanosystems, Daejeon, Korea) was used to measure and evaluate the mean width and mean thickness of the printed strain-gauge patterns.

2.4. Statistical Analysis

Minitab (version 20.1.3, Minitab, State College, PA, USA) was employed for statistical analysis. The Anderson–Darling test was used to determine the normality of data. Statistical significance was indicated by $p < 0.05$. Seven specimens were prepared for each topographical condition, and it was confirmed statistically that they conformed to a normal distribution.

3. Results and Discussion

Figure 3a illustrates the printed strain-gauge pattern on the PET substrate. The pattern was 7.76 mm in width and 13 mm in length. Seven samples were prepared for each topographical condition. The initial resistances of the printed strain-gauge patterns after sintering are depicted in Figure 3b. The resistance steadily decreased as the number of stacked layers or the width increased. The mean and standard deviation (SD) values of the resistance for each topographical condition are summarized in Table 1. The maximum percentage coefficient of variability, calculated as SD/mean × 100 (%CV), was 3.8% for the seven-droplet pattern. The minimum %CV was 1.6% for the two-droplet pattern. All %CV values were less than 5%, demonstrating the excellent reliability of the experimental dataset. In addition, normality was verified in the Anderson–Darling test for all datasets, as presented in Table 1 ($p > 0.05$).

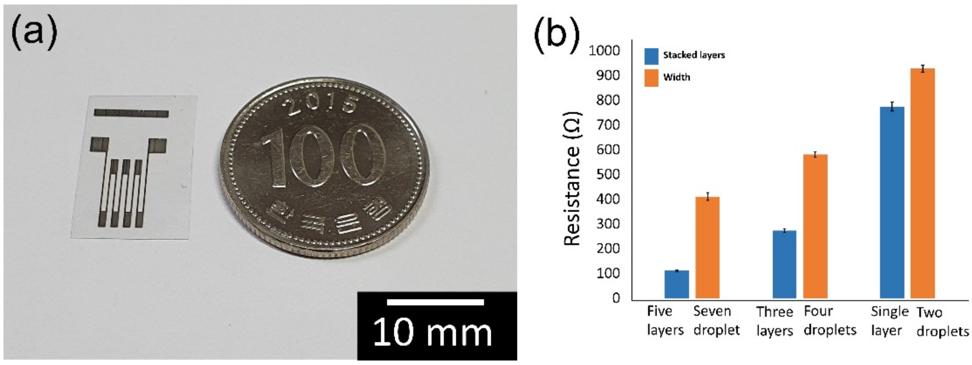

Figure 3. (**a**) Design of the printed strain gauge. (**b**) Resistance variations of the printed strain gauges. Blue and orange bars are for stacked layers and different widths, respectively. Data are mean and standard deviation values.

Table 1. Statistical evaluation of measured resistances of the printed strain-gauge patterns.

Topography		Mean (Ω)	SD (Ω)	%CV	p
Stacked layers	Five layers	111.04	3.08	2.8	0.136
	Three layers	273.23	8.21	3.0	0.639
	Single layer	774.00	18.36	2.4	0.069
Width	Seven droplets	410.87	15.52	3.8	0.304
	Four droplets	580.41	11.39	2.0	0.477
	Two droplets	927.78	15.02	1.6	0.687

SD, standard deviation; %CV, percentage coefficient of variability.

Figure 4 shows the cross-sectional profiles of the printed strain-gauge patterns. Figure 4a indicates that the thickness of the printed pattern was proportional to the number of stacked layers, and that the evenness of the pattern deteriorated for the five-layer pattern. It is assumed that the amount of evaporation was greater in the edge area of the deposited ink than in the central area, and that the resulting unbalanced evaporation forced the solute to move to the side area, producing a so-called coffee-ring effect [20,21]. The thickness of the coffee-ring stain superposed in the following printed layers. The peaks for single-, three- and five-layer patterns were 0.11934 µm, 0.32591 µm and 1.0 µm, respectively.

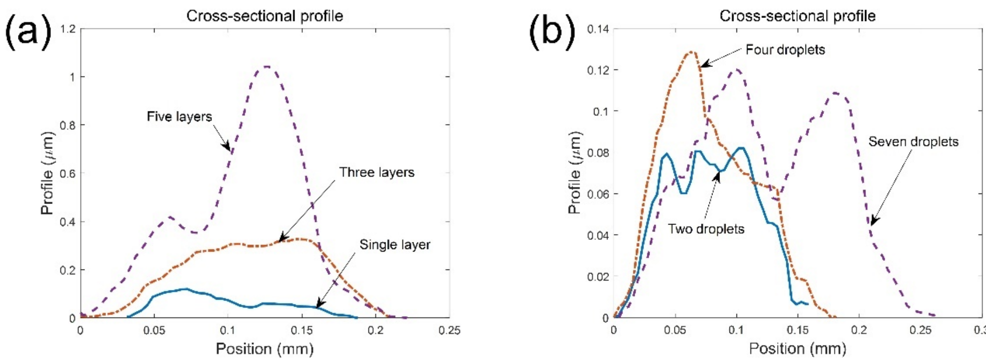

Figure 4. Cross-sectional profiles of printed strain-gauge patterns as a function of (**a**) the number of stacked layers and (**b**) the width.

Figure 4b illustrates the cross-sectional profiles of the printed strain-gauge patterns as a function of the numbers of droplets. The widths of the two-, four- and seven-droplet patterns with a fixed drop spacing of 30 µm were 144.87 µm, 176.19 µm and 264.29 µm, respectively. The width was not much smaller for two droplets than for four droplets, because the droplet could spread on the hydrophilic substrate to result in a compressed peak value of the width for the two-droplet pattern. In addition, the coffee-ring stain was clearly observed over the width of the seven-droplet pattern.

Figures 5 and 6 show interferometer images of printed strain-gauge patterns as functions of the number of stacked layers and the width, respectively. The size of the measured window was 1.1789 mm on the x-axis and 0.8846 mm on the y-axis for all images. In Figure 5, it is observed that the thickness of the printed pattern varied, and that the three-layer pattern was wider than the single-layer one. Figure 6 shows the distinct coffee-ring effect as the pattern widened. The mean widths and mean thicknesses of the strain-gauge patterns are summarized in Table 2.

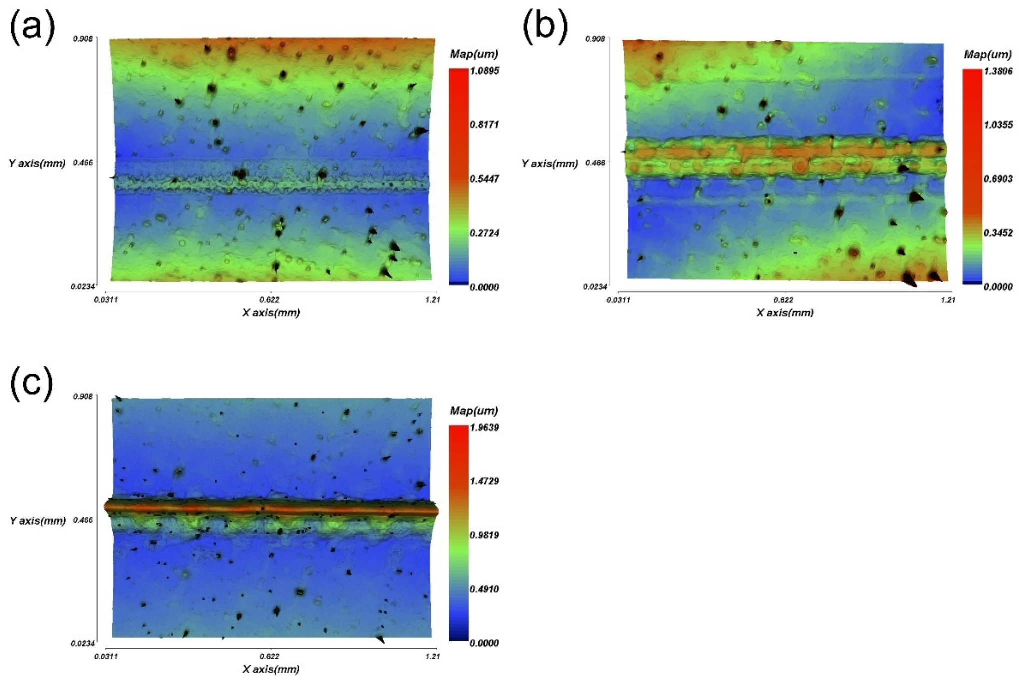

Figure 5. Interferometer images of printed strain gauges with stacked layers: (**a**) single layer, (**b**) three layers and (**c**) five layers.

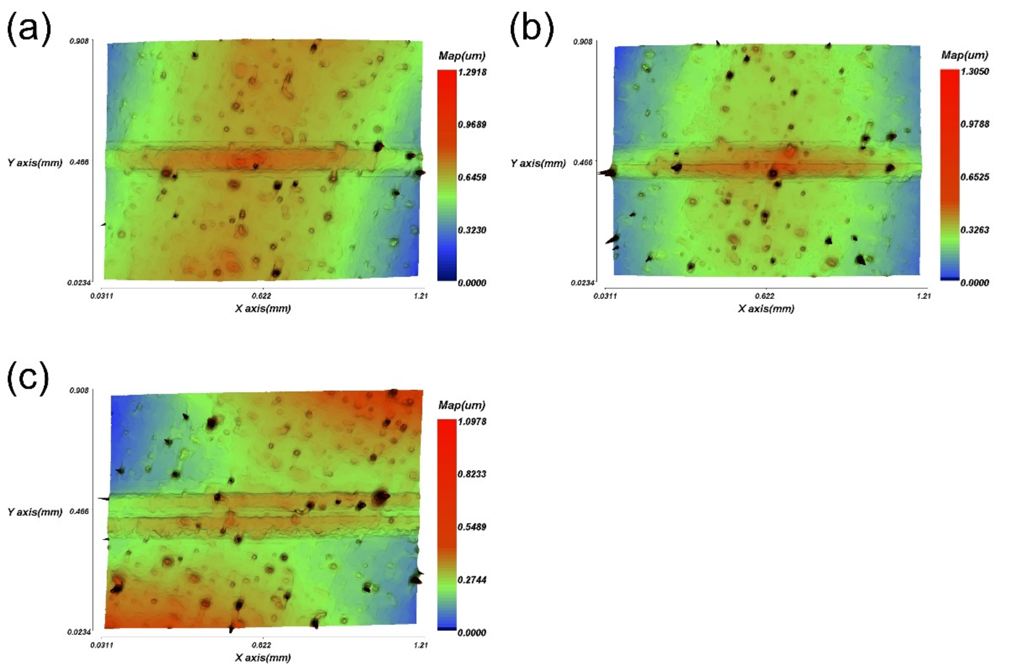

Figure 6. Interferometer images of printed strain gauges according to the pattern width: (**a**) two droplets, (**b**) four droplets and (**c**) seven droplets.

Table 2. Measured widths, thicknesses and corresponding gauge factors of printed strain-gauge patterns.

Topography		Mean Width (μm)	Mean Thickness (nm)	Area (μm^2)	Gauge Factor
Stacked layers	Five layers	209.39	404.36	84.67	3.098
	Three layers	203.15	175.08	35.57	3.051
	Single layer	163.34	63.52	10.37	2.471
Width	Seven droplets	266.60	62.12	16.56	2.589
	Four droplets	175.29	68.23	11.96	2.471
	Two droplets	151.59	58.42	8.86	2.047

The influence of the topography of the printed serpentine pattern on the sensitivity was investigated. The stacked-layer specimens were subjected to tensile stress in a bending test. The strains calculated using Equation (2) varied from 0.625‰ to 2.5‰. It was observed that the gauge factor increased from 2.471 to 3.098 as more layers were stacked, as shown in Figure 7. It was particularly interesting that the gauge factor also increased with the number of droplets, corresponding to an increased width. The gauge factor varied from 2.047 for two droplets to 2.589 for seven droplets, as shown in Figure 8.

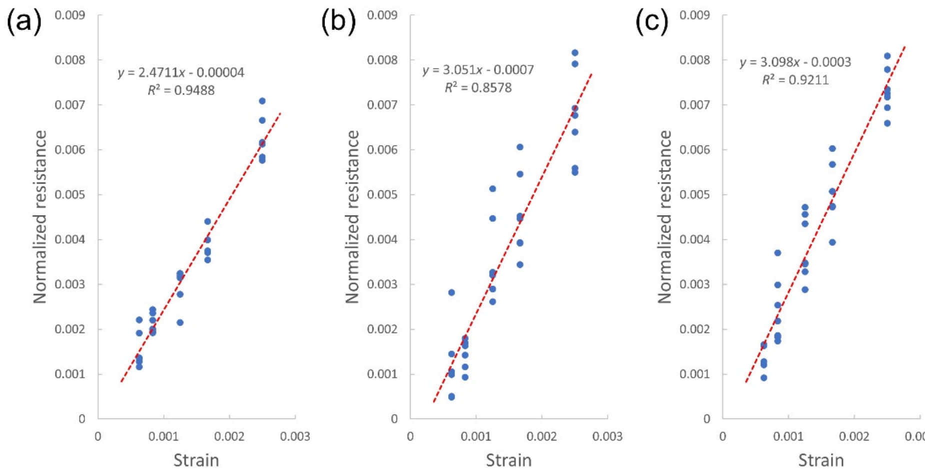

Figure 7. Gauge factor as a function of the number of stacked layers of printed strain-gauge patterns: (**a**) 2.471 for a single layer, (**b**) 3.051 for three layers and (**c**) 3.098 for five layers.

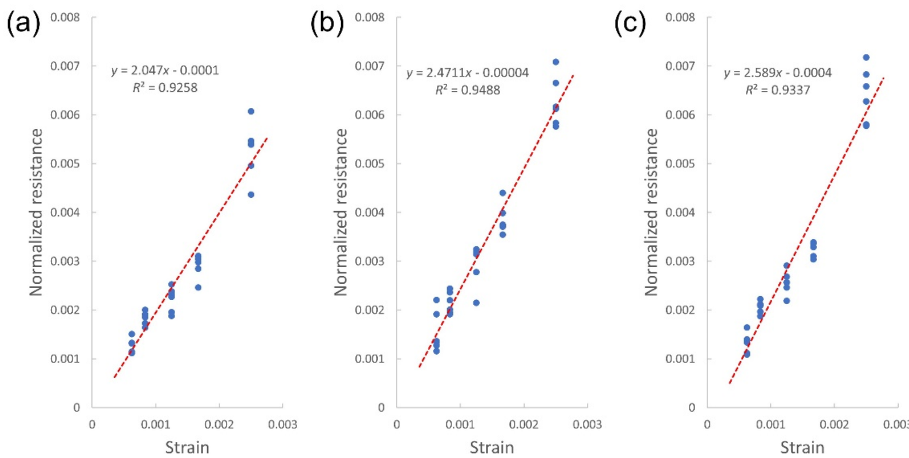

Figure 8. Gauge factor as a function of the width of printed strain-gauge patterns: (**a**) 2.047 for two droplets, (**b**) 2.471 for four droplets and (**c**) 2.589 for seven droplets.

The cross-sectional areas of the printed strain gauges and corresponding sensitivity factors are summarized in Table 2. Figure 9 shows that the gauge factor was proportional to the cross-sectional area of the printed strain-gauge pattern. The correlation was mathematically modelled as $y = 0.4167\ln(x) + 1.3837$, where x is the area in microns squared and y is the gauge factor. The coefficient of determination (R^2) was 0.8383.

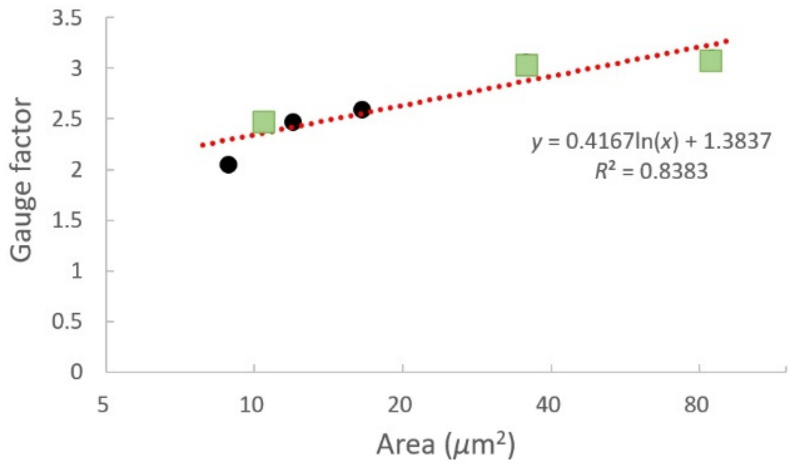

Figure 9. Gauge factor as a function of cross-sectional area of printed strain-gauge patterns. The black dots and green squares are for the width and the number of stacked layers, respectively.

The correlation between the geometrical variation in the conductive pattern and the gauge factor was mathematically derived based on some assumptions: (1) the geometrical deformation occurred in the linear elastic region and (2) the conductive pattern was isotropic. The resistance of the pattern with the initial geometry was calculated as

$$R = \rho_e({}^{L}/_{A}) = \rho_e({}^{L}/_{HW}) \tag{3}$$

The geometries were expressed using the following initial conditions and variations:

$$H = H_0 + \mathrm{d}H \tag{4}$$

$$W = W_0 + \mathrm{d}W \tag{5}$$

$$L = L_0 + \mathrm{d}L \tag{6}$$

where ρ_e is the specific electrical resistance, L, A, H and W are the length, cross-sectional area, height and width, respectively, and dL, dA, dH and dW are their corresponding variations. Then, the variation of resistance can be calculated as

$$\mathrm{d}R = R - R_0 = \rho_e \frac{(L_0 + \mathrm{d}L)}{(H_0 + \mathrm{d}H)(W_0 + \mathrm{d}W)} - \rho_e \frac{L_0}{H_0 W_0} \tag{7}$$

The strains within the cross section are

$$\varepsilon_w = {}^{\mathrm{d}W}/_{W_0},\ \varepsilon_H = {}^{\mathrm{d}H}/_{H_0} \tag{8}$$

Poisson's ratio yields

$$\nu = -{}^{\varepsilon_w}/_{\varepsilon_L} = -{}^{\varepsilon_H}/_{\varepsilon_L} \tag{9}$$

where ε_L, ε_w, ε_H and ν are the longitudinal strain, transverse strains for width and height, and Poisson's ratio, respectively.

Substituting Equation (8) into (7) gives

$$\mathrm{d}R = \rho_e \frac{L_0}{H_0 W_0}\left(\frac{1 + \varepsilon_L}{1 + \varepsilon_w + \varepsilon_H + \varepsilon_w \varepsilon_H} - 1\right) \tag{10}$$

Since $(\varepsilon_w + \varepsilon_H + \varepsilon_W \varepsilon_H) \ll 1$, Equation (10) can be rearranged as

$$\mathrm{d}R = \rho_e \frac{L_0}{H_0 W_0} (-\varepsilon_w - \varepsilon_H - \varepsilon_W \varepsilon_H + \varepsilon_L - \varepsilon_L \varepsilon_W - \varepsilon_L \varepsilon_H - \varepsilon_L \varepsilon_H \varepsilon_W) \tag{11}$$

Combining Equations (1), (9) and (11) gives

$$G_f = 1 + 2\nu + 2\nu \varepsilon_L - \nu^2 \varepsilon_L - \nu^2 {\varepsilon_L}^2 \tag{12}$$

Equation (12) indicates that the gauge factor can be determined from the longitudinal strain and Poisson's ratio of the conductive pattern. To compare the gauge factors measured experimentally, we used a strain of 2.5‰ and Poisson's ratio for bulk Ag of 0.37. This yielded a gauge factor of 1.742, which was lower than the measured range from 2.047 to 3.089, as indicated in Table 2. We could speculate that this discrepancy in gauge factor is attributed to the porosity of sintered printed Ag layer. In [22], the porosity of material influences tensile mechanical properties, e.g., elastic modulus, ultimate strength, and elongation. Then, the porosity could affect the gauge factor as well as Poisson's ratio of sintered Ag layer in Equations (9) and (12). Moreover, the anisotropy of the sintered Ag layer, which was characterized by different lateral and longitudinal deformations, could markedly reduce the electrical conductivity [23,24]. In further study, we will investigate the correlation between porosity and gauge factor in microstructure investigation.

4. Conclusions

In this study, we performed a topographical analysis of inkjet-printed strain gauges produced using Ag on a PET substrate. Serpentine strain-gauge sensor patterns were fabricated using DOD inkjet printing, and the deposited patterns were sintered in a conventional convection oven at 150 °C for 15 min to ensure high conductivity. For the parametric investigation, the strain-gauge patterns were printed with variations in thickness, from 58.42 nm to 404.3 nm, and in width, for 151.59 µm to 209.39 µm. To calculate the gauge factor, the fabricated strain-gauge sensor was attached to curved surfaces for bending tests. The obtained gauge factors ranged from 2.047 to 3.098, and were proportional to the cross-sectional area of the printed strain-gauge pattern. The correlation was mathematically modelled as $y = 0.4167\ln(x) + 1.3837$, with an R^2 of 0.8383.

The analysis results indicated that the gauge factor of the inkjet-printed strain-gauge sensor can be modified by controlling the cross-sectional area of the gauge pattern without changing its serpentine shape. This represents a highly useful feature for an inkjet-printed strain-gauge sensor with a controllable gauge factor.

Author Contributions: Conceptualization, H.K.; Data Curation, J.S.; Formal Analysis, H.K. and S.K. (Seokjin Kim); Writing—Original Draft Preparation, H.K.; Writing—Review and Editing, H.K. and S.K. (Sunglim Ko). All authors have read and agreed to the published version of the manuscript.

Funding: This paper was supported by the Konkuk University in 2019.

Conflicts of Interest: The authors declare that they have no known competing financial interests or personal relationships that could have appeared to influence the work reported in this paper.

References

1. Albert, E.B. The Structures of Strain Gauge Transducers: An Introduction. *IEEE Trans. Ind. Appl.* **1969**, *5*, 90–94.
2. Vinogradov, R.I. Strain-gauge pressure transducers of a new design. *Meas. Tech.* **1962**, *5*, 471–474. [CrossRef]
3. Khan, S.; Ali, S.; Khan, A.; Ahmed, M.; Wang, B.; Bermak, A. Inkjet printing of multi-stripes based deflection monitoring sensor on flexible substrate. *Sens. Actuators A Phys.* **2021**, *323*, 112638. [CrossRef]
4. Anderson, N.; Szorc, N.; Gunasekaran, V.; Joshi, S.; Jursich, G. Highly sensitive screen printed strain sensors on flexible substrates via ink composition optimization. *Sens. Actuators A Phys.* **2019**, *290*, 1–7. [CrossRef]
5. Li, S.; Park, J.G.; Wang, S.; Liang, R.; Zhang, C.; Wang, B. Working mechanisms of strain sensors utilizing aligned carbon nanotube network and aerosol jet printed electrodes. *Carbon* **2014**, *73*, 303–309. [CrossRef]

6. Bisconti, F.; Giuri, A.; Suhonen, R.; Kraft, T.M.; Ylikunnari, M.; Holappa, V.; Po, R.; Biagini, P.; Savoini, A.; Marra, G.; et al. One-step polymer assisted roll-to-roll gravure-printed perovskite solar cells without using anti-solvent bathing. *Cell Rep. Phys. Sci.* **2021**, *2*, 100639. [CrossRef]
7. Park, J.; Nam, D.; Park, S.; Lee, D. Fabrication of flexible strain sensors via roll-to-roll gravure printing of silver ink. *Smart Mater. Struct.* **2018**, *27*, 085014. [CrossRef]
8. Yi, Y.; Wang, B.; Bermak, A. A low-cost strain gauge displacement sensor fabricated via shadow mask printing. *Sensors* **2019**, *19*, 4713. [CrossRef]
9. Enser, H.; Kulha, P.; Sell, J.K.; Michaela, S.L.; Strauß, B.; Hilber, W.; Jakoby, B. Printed strain gauges embedded in organic coatings—Analysis of gauge factor and temperature dependence. *Sens. Actuators A Phys.* **2018**, *276*, 137–143. [CrossRef]
10. Borghetti, M.; Serpelloni, M.; Sardini, E.; Casas, O. Multisensor System for Analyzing the Thigh Movement During Walking. *IEEE Sens. J.* **2017**, *17*, 4953–4961. [CrossRef]
11. Shakeel, M.; Khan, W.A.; Rahman, K. Fabrication of cost effective and high sensitivity resistive strain gauge using DIW technique. *Sens. Actuators A Phys.* **2017**, *258*, 123–130. [CrossRef]
12. Zhang, Z.; Si, T. Controllable assembly of silver nanoparticles based on the coffee-ring effect for high-sensitivity flexible strain gauges. *Sens. Actuators A Phys.* **2017**, *264*, 188–194. [CrossRef]
13. Ali, M.M.; Maddipatla, D.; Narakathu, B.B.; Chlaihawi, A.A.; Emamian, S.; Janabi, F.; Bazuin, B.J.; Atashbar, M.Z. Printed strain sensor based on silver nanowire/silver flake composite on flexible and stretchable TPU substrate. *Sens. Actuators A Phys.* **2018**, *274*, 109–115.
14. Barmpakos, D.; Tsamis, C.; Kaltsas, G. Multi-parameter paper sensor fabricated by inkjet-printed silver nanoparticle ink and PEDOT:PSS. *Microelectron. Eng.* **2020**, *225*, 111266.
15. Zymelka, D.; Yamashita, T.; Takamatsu, S.; Itoh, T.; Kobayashi, T. Printed strain sensor with temperature compensation and its evaluation with an example of applications in structural health monitoring. *Jpn. J. Appl. Phys.* **2017**, *56*, 05EC02. [CrossRef]
16. Guo, Z.; Xu, J.; Chen, Y.; Guo, Z.; Yu, P.; Liu, Y.; Zhao, J. High-sensitive and stretchable resistive strain gauges: Parametric design and DIW fabrication. *Compos. Struct.* **2019**, *223*, 110955. [CrossRef]
17. Enser, H.; Sell, J.K.; Hilber, W.; Jakoby, B. Printed strain sensors in organic coatings: In depth analysis of sensor signal effects. *Sens. Actuators A Phys.* **2018**, *281*, 258–263. [CrossRef]
18. Zhang, Y.; Anderson, N.; Bland, S.; Nutt, S.; Jursich, G.; Joshi, S. All-printed strain sensors: Building blocks of the aircraft structural health monitoring system. *Sens. Actuators A Phys.* **2017**, *253*, 165–172. [CrossRef]
19. Hibbeler, R.C. *Mechanics of Materials*, 8th ed.; Pearson Prentice Hall: Hoboken, NJ, USA, 2011; pp. 281–294.
20. Deegan, R.D.; Bakajin, O.; Dupont, T.F.; Huber, G.; Nagel, S.R.; Witten, T.A. Capillary flow as the cause of ring stains from dried liquid drops. *Nature* **1997**, *389*, 827–829. [CrossRef]
21. Soltman, D.; Subramanian, V. Inkjet-Printed Line Morphologies and Temperature Control of the Coffee Ring Effect. *Langmuir* **2008**, *24*, 2224–2231. [CrossRef]
22. Su, S.; Rao, Q.; He, Y.; Xie, W. Effects of porosity on tensile mechanical properties of porous FeAl intermetallics. *Trans. Nonferr. Met. Soc. China* **2020**, *30*, 2757–2763. [CrossRef]
23. Chen, J.; Liu, X.; Tian, Y.; Zhu, W.; Yan, C.; Shi, Y.; Kong, L.B.; Qi, H.J.; Zhou, K. 3D-Printed Anisotropic Polymer Materials for Functional Applications. *Adv. Mater.* **2021**, *34*, 2102877. [CrossRef] [PubMed]
24. Maroti, P.; Varga, P.; Abraham, H.; Falk, G.; Zsebe, T.; Meiszterics, Z.; Mano, S.; Csernatony, Z.; Rendeki, S.; Nyitrai, M. Printing orientation defines anisotropic mechanical properties in additive manufacturing of upper limb prosthetics. *Mater. Res. Express* **2019**, *6*, 035403. [CrossRef]